Geophysical Research Letters

RESEARCH LETTER
10.1002/2018GL077354

Special Section:
Cassini's Final Year: Science Highlights and Discoveries

Analysis of Intense *Z*-Mode Emission Observed During the Cassini Proximal Orbits

J. D. Menietti[1], T. F. Averkamp[1], S.-Y. Ye[1], A. H. Sulaiman[1], M. W. Morooka[2], A. M. Persoon[1], G. B. Hospodarsky[1], W. S. Kurth[1], D. A. Gurnett[1], and J.-E. Wahlund[2]

[1]Department of Physics and Astronomy, University of Iowa, Iowa City, IA, USA, [2]Swedish Institute of Space Physics, Uppsala, Sweden

Key Points:
- Intense *Z*-mode emission is observed along Saturn proximal orbits down to and within the ionosphere
- Source regions may be along magnetic field lines that thread SKR source regions or along inner edge of Enceladus torus
- *Z* mode may interact with electrons to fill or deplete the inner radiation belts

Correspondence to:
J. D. Menietti,
john-menietti@uiowa.edu

Citation:
Menietti, J. D., Averkamp, T. F., Ye, S.-Y., Sulaiman, A. H., Morooka, M. W., Persoon, A. M., et al. (2018). Analysis of intense *Z*-mode emission observed during the Cassini proximal orbits. *Geophysical Research Letters*, *45*, 6766–6772. https://doi.org/10.1002/2018GL077354

Received 29 JAN 2018
Accepted 9 MAR 2018
Accepted article online 14 MAR 2018
Published online 28 JUN 2018

Abstract The role of *Z*-mode emission in the diffusive scattering and resonant acceleration of electrons is believed to be important at Saturn. A survey of the "5 kHz" component of this emission at Saturn earlier reported strong intensity in the lower density regions where the ratio of plasma frequency to cyclotron frequency, $f_p/f_c < 1$. At Saturn this occurs along the inner edge of the Enceladus torus near the equator and at higher latitudes. Using the Cassini Radio and Plasma Wave Science instrument observations during the Cassini proximal orbits, we have now identified these emissions extending down to and within the ionosphere. Wave polarization measurements and unique frequency cutoffs are used to positively identify the wave mode. Analogous to the role of whistler mode chorus at Earth, Saturn *Z*-mode emissions may interact with electrons contributing to the filling or depleting of Saturn's inner radiation belts.

Plain Language Summary Very intense waves are observed near Saturn that have been identified as *Z* mode. These waves are unusual because they are observed in a narrow range of frequencies from uncertain source regions and generation mechanism. However, we know that these waves can scatter electrons or even accelerate them by a process that is observed at Earth due to similar waves (whistler mode chorus), causing the terrestrial radiation belts to fill with high energy electrons or to dump those electrons along magnetic field lines toward the polar auroral regions. At Saturn *Z*-mode waves may be a source of filling or depleting Saturn radiation belts that lie along magnetic field lines that are intercepted by the waves. We have used the Cassini wave instrument to measure wave properties such as polarization and unique wave cutoff frequencies to positively identify these waves along the orbit of Cassini extending from the polar auroral regions down to closest approach within the Saturn ionosphere.

1. Introduction

Whistler mode chorus emission is known to play a significant role in filling the Earth's radiation belts by radial diffusion and local electron acceleration (cf. Baker et al., 2013; Horne et al., 2005; Reeves et al., 2013; Shprits, Elkington, et al., 2008; Shprits, Subbotin, et al., 2008). Similar electron gyro-resonant models of chorus wave-particle interactions at Jupiter have also been introduced (i.e., Horne et al., 2008; Katoh et al., 2011; Woodfield et al., 2014). At Saturn, however, the role of chorus in the filling of radiation belts is not as definitive (Shprits et al., 2012). Recent discoveries of intense *Z*-mode radiation at Saturn (not similarly observed at Earth) suggest a new scenario for wave-particle interactions in the Kronian magnetosphere. *Z*-mode observations during the Cassini proximal orbits are particularly intense.

Z-mode emission is "trapped" electromagnetic emission that propagates between the lower frequency cutoff $f_z = \frac{1}{2}\left(\sqrt{f_c^2 + 4f_p^2} - f_c\right)$ and the upper hybrid frequency resonance$f_{uh} = \sqrt{f_c^2 + f_p^2}$ where f_c is the electron cyclotron frequency and f_p is the electron plasma frequency, respectively. The role of *Z* mode in the acceleration of radiation belt electrons has been discussed in the past by Horne and Thorne (1998), Glauert and Horne (2005), and Albert (2007). Ye et al. (2010) have reported significant intensities of *Z*-mode emission at Saturn in the low-density region near the inner edge of the Enceladus plasma torus ranging from just above the equator to higher latitudes. The latter authors classified these narrowband emissions, which occur in two general bands, as "5 kHz" and "20 kHz" emission. Gu et al. (2013), using *Z*-mode observations of Saturn narrowband *Z*-mode emissions, computed bounced-averaged diffusion coefficients for Saturn radiation belt electrons. The authors found that the 5 kHz emission can cause resonant scattering of electrons in the range from a few MeV to tens of MeV, while the 20 kHz waves resonate from a few hundreds of keV to several MeV. Recently, Woodfield et al. (2016) have presented results of stochastic modeling of electron scattering by

chorus and *Z* mode in the Saturn magnetosphere. Their results indicate that chorus alone does not fully explain the electron fluxes observed in the inner kronian magnetosphere. They further indicate that the influence of *Z*-mode emission observed in the inner magnetosphere inside the orbit of Enceladus may be sufficient to explain the observed electron fluxes filling the radiation belt in the inner magnetosphere of Saturn.

Subsequent to the work of Ye et al. (2010), Menietti et al. (2015) reported a survey of the intensity of 5 kHz *Z* mode and obtained parametric fits relative to frequency, radius, latitude, and local time. At the time no observations of the Saturn magnetosphere for $r < 2.5$ R_s had been made except during the orbit injection of Cassini. The narrow band 5 kHz emission usually is more intense than the 20 kHz emission, and both bands are observed to have mixtures of both *Z* and *O* modes. In regions outside the outer radius of the Enceladus torus, where f_c falls below 5 kHz, narrowband emission can only propagate in the ordinary (*O*). For the inner region at distances less than the inner radius of the Enceladus torus, where $f_p/f_c < 1$, however, both *Z* mode and *O* mode can propagate for $f > f_p$, whereas for $f < f_p$, only the *Z* mode can propagate. When the wave frequency is greater than f_p, *Z* mode is right-hand (RH) polarized, while for $f < f_p$, *Z* mode is left-hand (LH) polarized (Benson et al., 2006). *O* mode is LH polarized.

Starting on 26 April 2017, a series of 22 orbits, each with an inclination of 61.7° and a periapsis of ~1.06 R_s, was flown by Cassini. During a number of these orbits, the Radio and Plasma Wave Science (RPWS) instrument onboard Cassini observed intense emission identified as *Z* mode. Polarization measurements as well as the known properties of the plasma modes relative to f_p and f_c are used to identify the emission. In addition, we use direction finding measurements from the High Frequency Receiver of the RPWS (cf. Cecconi & Zarka, 2005) to place constraints on the *Z*-mode source region. Finally, we estimate the wave normal angle of the observed *Z*-mode emission based on the measured polarization and cold plasma magnetosonic theory. Since *Z* mode can be an efficient source of electron scattering and trapping of electrons to fill the radiation belts, these observations will be of significant interest to the planetary community. Intense *Z* mode at high occurrence probability is not seen at Earth, making these observations unique to the solar system at the present time.

2. Methodology

The Cassini RPWS instrument is the source of the plasma and radio wave observations reported in this study. The instrument has three low-time resolution receivers, the low (LFR, 1–26 Hz), medium (MFR, 24 Hz – 12 kHz), and high (HFR, 3.5 kHz–16 MHz). The *Z* mode is observed almost exclusively by the HFR. There are three approximately orthogonal electric antennas and three orthogonal search coils. The HFR obtains autocorrelation and cross-correlation measurements from two selected antennas. These are used in ground processing to provide direction of arrival information and all four Stokes parameters. The frequency resolution in the low-rate data is $\Delta f/f \sim 7\%$. A high-resolution wideband receiver covers two frequency bands, 60 Hz to 10.5 kHz and 800 Hz to 74 kHz. See Gurnett et al. (2004) for a complete description of the RPWS instrument.

The RPWS also measures the wave polarization via the HFR data. Fischer et al. (2009) and Ye et al. (2010) gave a thorough description of the real and apparent polarization of radio waves measured with the HFR. The RPWS instrument can operate in either the two-antenna or the three-antenna mode. The three-antenna mode uses three monopole antennas to perform direction finding, while the two-antenna mode operates in a dipole-monopole (or polarimeter) configuration. Fischer et al. (2009) and Ye et al. (2010) discussed the apparent polarization of radio emission, assuming the antenna plane and the wave plane are parallel. Knowing the direction to the source of the emission allows for a linear transformation to calculate the real polarization (Galopeau et al., 2007; Hamaker et al., 1996). This requires the instrument to be in the three-antenna mode. We rely on both the apparent and actual polarization (in the plasma convention) to help identify the wave modes observed. The apparent polarization is calculated from the apparent Stokes parameters (cf. Ye et al., 2010, equations 1–4), which are normalized to the apparent Poynting flux. The apparent circular polarization degree is defined as $d_{c,app} = v_{app}$, with -1 (right circular polarization) $\le v_{app} \le +1$ (left circular polarization) if the incident wave is received on a specific side of the antenna plane. The apparent polarization degree is defined as $d_{app} = \sqrt{q_{app}^2 + u_{app}^2 + v_{app}^2}$, with $d_{app} = 0$, 0.5, and 1.0 (unpolarized, partially polarized, and completely polarized). It is necessary to know on which side of the antenna plane the incident wave

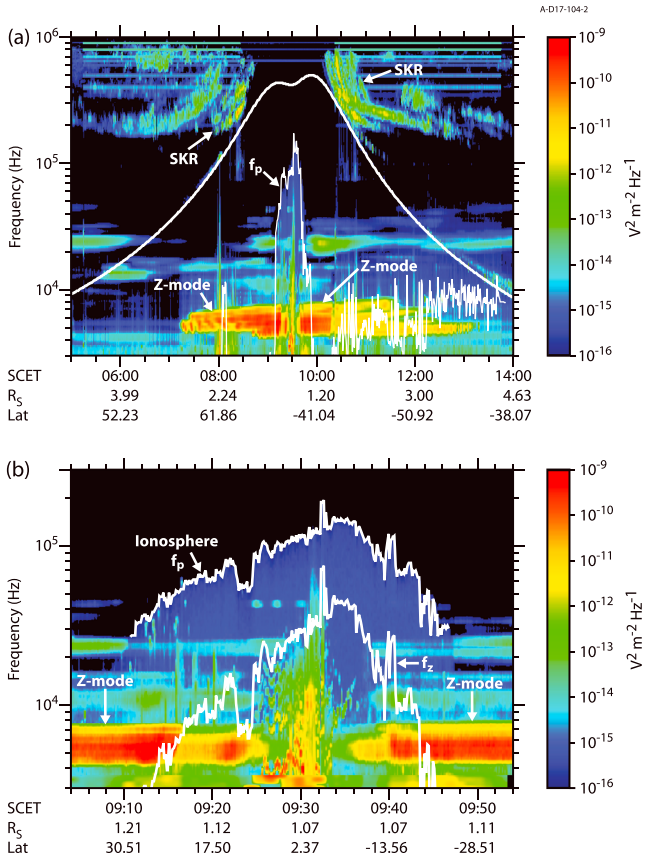

Figure 1. (a) A frequency-versus-time spectrogram during the periapsis pass of day 187 of 2017 on proximal orbit 282. Electric spectral density is (color-coded), with intense *Z*-mode emission and Saturn kilometric emission indicated on the plot. *Z*-mode emission is narrowbanded in the approximate frequency range 5 kHz $< f <$ 7 kHz and is located on both sides of the magnetic equator/ring plane, which is crossed near 09:30. (b) A higher resolution spectrogram of the emission in the region near perikrone, including the ring plane crossing within the ionosphere.

arrives, which is dependent on the sign of the angle β, the elevation of the radio source with respect to the antenna plane (cf. Fischer et al., 2009).

3. Saturn *Z*-Mode Observations and Analysis

Figure 1a is a frequency-versus-time spectrogram during the periapsis pass of day 187 of 2017 on proximal orbit 282. Seen on the spectrogram are electric spectral densities (color-coded), with intense *Z*-mode emission and Saturn kilometric radiation (SKR) indicated on the plot. *Z*-mode emission is narrowbanded in the approximate frequency range 5 kHz $< f <$ 7 kHz and is located on both sides of the magnetic equator/ring plane, which is near 09:30. This morphology has been observed on numerous high inclination orbits of Cassini as reported by Ye et al. (2010) and Menietti et al. (2015). The emission is most intense near the equator at radial distances less than the inner radius of the Enceladus plasma torus within about 2.5 R_s. Since the Cassini orbital insertion on 1 July 2004 (Gurnett et al., 2005) no observations near the equator at radial distances $\lesssim 2.5R_s$ have occurred until the proximal orbits. Also shown on this plot are the cyclotron frequency (upper smooth white line) and the electron plasma frequency (lower more erratic white line). For most of the time in the northern hemisphere f_p is less than 3 kHz.

When the Cassini spacecraft is near a source region of SKR, the local cyclotron frequency is close to the lower cutoff of the SKR emission, which is believed to be generated by the cyclotron maser instability (Wu & Lee, 1979). This happens twice during the periapsis pass of Figure 1, once in the northern hemisphere in the approximate interval 08:20 to 08:40 and more nearly in the southern hemisphere in the approximate interval 10:10 to 10:50. The plasma frequency at higher latitudes is obtained from the Langmuir Probe (LP) "proxy" data (Wahlund et al., 2005). The LP floating potential is used as a proxy for the number density in a tenuous plasma (Morooka et al., 2009). This calculation is limited to regions of $n_e < 5$ cm^{-3}, generally. Within the high density ionosphere, f_p can be calculated using the LP "sweep mode" (Wahlund et al., 2018) or the whistler mode high-frequency cutoff obtained from the RPWS instrument (Persoon et al., 2018).

Figure 1b shows a higher resolution spectrogram of the emission in the region near perikrone, including the ring plane crossing within the ionosphere. The Saturn ionosphere has been first identified by Wahlund et al. (2018), and we indicate the boundary of this region by the upper cutoff of whistler mode emission at the plasma frequency. Knowing f_p as well as f_c, we can calculate f_z, indicated on both sides of the magnetic equator crossing. This cutoff corresponds exactly to the low-latitude boundary of the observed emission in the northern hemisphere between approximately 09:14 and 09:16, where there is a distinct decrease in wave spectral density for $f < f_z$. This is consistent with identification of *Z*-mode emission at higher latitude, and probably whistler (*W*) mode for the region at lower latitude as discussed in Sulaiman et al. (2017). The whistler mode can only propagate at $f < f_p$ for $f_p/f_c < 1$. The *Z*-mode emission at higher northern latitude is more intense and somewhat larger in bandwidth than the emission south of the ring plane. In the southern hemisphere there is a boundary at f_z near 09:43–09:44 with *Z* mode at higher southern latitudes where $f > f_z$ and probably *W* mode for $t <$ 09:43, near the ring plane. Near the f_z boundaries in the northern and southern hemispheres (~09:15, ~09:43, respectively) there is evidence of strong wave refraction (shown later) and so there is a possibility of wave mode conversion (*Z* mode to *W* mode).

The Poynting flux and polarization of the waves are shown in Figures 2a and 2b for the time period when Cassini was outside the ring plane crossing region ($t \lesssim$ 08:30, $t \gtrsim$ 10:30) and the HFR receiver was in the three-antenna mode. For three-antenna measurements polarization and direction finding are possible. There remains a 180° uncertainty in the source direction, either approaching or receding from the antenna plane. If the polarization is known to be either RH or LH, this uncertainty is removed. Closest to the ring

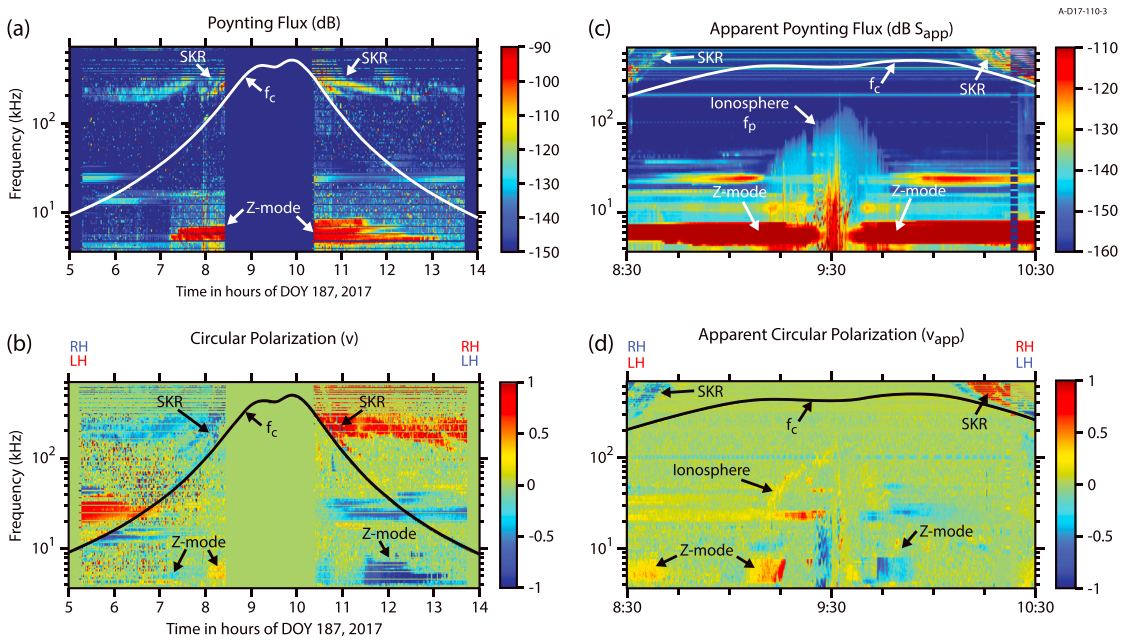

Figure 2. The (a) Poynting flux and (b) polarization of the waves for the time period when Cassini was outside the ring plane crossing region ($t \lesssim$ 08:30, $t \gtrsim$ 10:30). (c) Apparent Poynting flux and (d) apparent polarization for the period closest to the ring plane crossing when only two-antenna mode data are available.

plane crossing only two-antenna mode data are available, and we display the apparent Poynting flux and polarization in Figures 2c and 2d. The polarization is determined by cross correlation of the antenna signals of the HFR antennas and is dependent on the evaluation of **k** • **B**, where **k** is the wave vector and **B** is the ambient magnetic field. Note that the color used to designate polarization handedness changes as the spacecraft crosses the ring plane (RH becomes RH and LH becomes LH). This is because the source directions vary in each hemisphere. The emission labeled *Z* mode in Figure 2d appears blue for north of the ring plane and red for south of the ring plane, consistent with *Z*-mode emission LH circular polarization when the wave frequency is less than f_p. The polarization of the whistler mode (*W*) emission north of the ring plane is measured to be very low, as is much of the *Z*-mode emission between ~8:40 and ~9:10 perhaps due to the orientation of the HFR antenna or signal quality. In the region ~09:10 $< t <$ 09:15 the polarization is left-handed and the emission frequency is less than f_p (see Figure 1), which is consistent with *Z* mode. The change in color from blue to red across the ring plane is consistent with a different source region (direction) measured by the HFR. Note that the *Z* mode in the region ~09:44 $< t \lesssim$ 09:54 is seen as red/yellow (LH) for $f < f_p$, while RH whistler mode is blue, consistent with a different source region south of the ring plane (**k** • **B** $<$ 0). For $t \gtrsim$ 09:55 the measured polarization of *Z*-mode emission is almost zero. At higher latitude in Figure 2a (and Figure 1) we note a region of higher density in the approximate interval 08:05 $< t <$ 08:20 as determined by the LP. This region is associated with the SKR source in the northern hemisphere and may also be indicated by enhanced lower frequency whistler mode waves (Figure 1) that extend upward in frequency. Both *Z* and *W* modes are possible in this region, but *Z* mode would be LH polarized (red) and *W* mode would be RH polarized (blue) for $f < f_p$. The yellow-red color extending from ~08:05 $< t <$ 08:30, 5 kHz $< f <$ 7 kHz (Figure 2b) indicates probable dominance of *Z* mode in this region. The southern hemisphere 5 kHz emission for $t >$ 10:30 is dominantly blue indicating *Z* mode except in the region between ~10:50 $< t <$ 11:20, where the polarization is near zero. This latter region is associated with the southern hemisphere SKR source region where, as is the case of the northern hemisphere, we see an increase of density as measured by the LP and

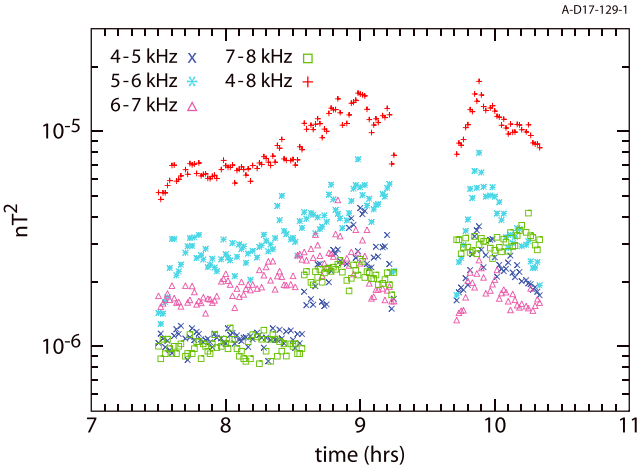

Figure 3. *Z*-mode intensity for specific frequency ranges. These data are obtained from the magnetic search coil.

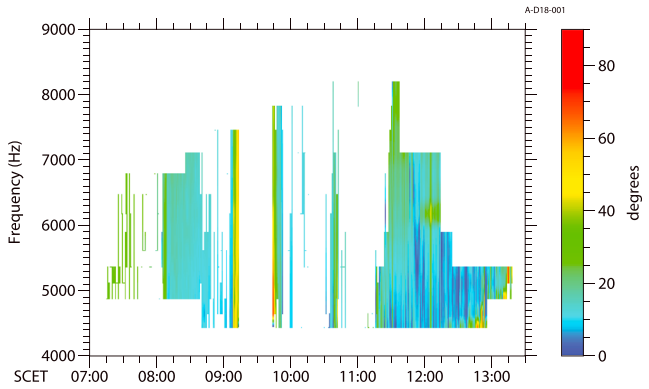

Figure 4. Wave normal angles of the *Z*-mode emission are modeled using cold plasma theory. Most of these wave normal angles are less than ~25°.

enhanced lower frequency *W* mode, which has opposite polarization from *Z* mode in this region.

In Figure 3 we plot the *Z* mode intensity for specific frequency ranges for this perikrone pass. These data are obtained from the magnetic search coil, which has higher relative noise level than the electric field data in this frequency range, and emission is observed for a smaller range of frequency and time than the electric field data shown in Figure 1. We note that these *Z*-mode intensities are among the highest observed by Cassini RPWS instrument for any orbits prior to the proximal orbits.

The wave normal angles (between **k** and **B**) of the *Z*-mode emission are modeled using cold plasma theory, which is suitable for the magnetosphere and upper ionosphere of Saturn. In this approximation the wave polarization relative to the wave vector is given by equation (52) (Stix, 1992, p. 22) as

$$\frac{iE_a}{E_b} = \frac{(n^2 - S)P\cos\theta}{D\left(P - n^2\sin^2\theta\right)} = \frac{Sn^2 - RL}{Dn^2\cos\theta}$$

where E_a and E_b are orthogonal components of the wavefield and *S*, *P*, *R*, *L*, and *D* are the Stokes parameters. Calculated values are plotted in Figure 4. Most of these wave normal angles are less than ~25°.

In Figure 5 we present analysis of the RPWS HFR direction finding results for the emissions in the frequency range approximately 5 to 7.5 kHz. We display results in the *z*-*x* plane for Saturn equatorial coordinates, which are defined as *x* in the Saturn-Sun plane, +*x* toward the Sun, +*z* along the Saturn northern spin axis, and *y* given by **z** × **x**. The spacecraft trajectory is shown in red, and the direction to the source region is indicated by a blue arrow. The number of vectors has been reduced for presentation, but some locations have very few or no vectors due to low signal-to-noise ratio or uncertain or small value of polarization (Stokes parameter, *v*). The vectors are drawn only for *Z* mode during the times shown. We have labeled the times when Cassini traversed magnetic field lines along which lie SKR source regions. During these times in both the northern and southern hemispheres, it is believed that Cassini is just above the SKR source region. The vectors during these times are directed toward Saturn, consistent with a *Z*-mode source lying along magnetic field lines that thread the SKR source region. Near the ring plane and magnetic equator crossing we observe an interesting reflection or refraction effect in both the northern and southern hemispheres near the entry and exit of the ionosphere. The spacecraft is very close to the Saturn surface at this time. It is possible that a *Z*-mode source region is below Cassini, but it may also be that the source region is actually 180° opposite the vector direction at this time, and points away from Saturn. These rays from the northern and southern hemispheres may intersect near 2.5 R_s as indicated by the dashed lines in Figure 5. The other bundles of rays (indicated "R" in the figure) near the ionosphere could represent those rays reflected and refracted from the ionosphere near the *L* = 0 cutoff of *Z* mode.

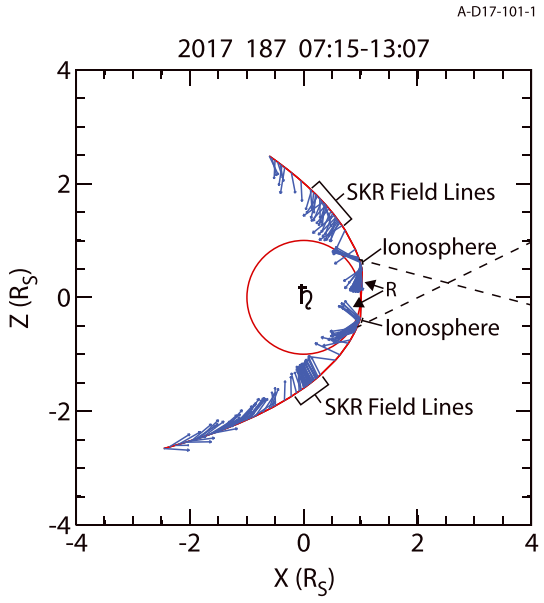

Figure 5. Direction finding results for the *Z* mode in the frequency range approximately 5 to 7.5 kHz. We display results in the *z*-*x* plane for Saturn equatorial coordinates (defined in the text). The spacecraft trajectory is shown in red, and the direction to the source region is indicated by a blue arrow.

4. Summary and Conclusions

The proximal orbits provide a unique opportunity for the Cassini spacecraft to observe plasma waves in a previously unexplored region including the ionosphere near the ring plane. Encounters with magnetic field lines threading SKR source regions were frequent along these orbits. A combination of wave analysis tools including polarization and direction finding observations were utilized in this study. These tools along with plasma density measurements allowing the identification of f_z, the low-frequency cutoff of *Z* mode, have facilitated the identification of intense narrowband *Z*-mode emission in the frequency range ~4 < *f* < 8 kHz down to and

within the Saturn ionosphere. The propagation range extends from $\lambda \gtrsim 10°$. Intense *Z*-mode emissions are known to exist at lower latitudes in the low-density region extending inward from ~4.0 R_s to ~2.5 R_s (cf. Menietti et al., 2015; Ye et al., 2010). The wave normal angles (between **k** and **B**) appear to be relatively small, with the majority of values $\lesssim 25°$. The observations presented in the present study imply that these waves are likely to be observed extending inward to and within Saturn's ionosphere.

Direction finding analysis implies that source regions for these emissions may be along magnetic field lines that thread SKR source regions. However, source regions at low-latitude perhaps within the ionosphere or at larger radial distances cannot be ruled out. Regions of strong wave refraction near the f_z boundary in each hemisphere are also indicated, and these could be regions of wave mode conversion.

Z-mode emissions at Saturn have been shown to be important in pitch angle and momentum scattering of electrons in the energy range hundreds of keV $< E <$ 2 MeV (Gu et al., 2013; Woodfield et al., 2016), and they may be important in the process of filling or depleting the Saturn inner radiation belts.

Acknowledgments
We thank J. Barnholdt for administrative assistance and J. Chrisinger for help with the figures. J. D. M. acknowledges support from JPL contract 11415150 and NASA grants NNX16AI47G and NNX11AM36G. Cassini RPWS data are scheduled to be archived in calibrated, full resolution at the NASA Planetary Data System website: http://pds.nasa.gov/, or are available upon request from J. D. M.

References

Albert, J. M. (2007). Refractive index and wavenumber properties for cyclotron resonant quasilinear diffusion by cold plasma waves. *Physics of Plasmas*, *14*(7), 072901. https://doi.org/10.1063/1.2744363

Baker, D. N., Kanekal, S. G., Hoxie, V. C., Henderson, M. G., Li, X., Spence, H. E., et al. (2013). A long-lived relativistic electron storage ring embedded in Earth's outer Van Allen Belt. *Science*, *340*(6129), 186–190. https://doi.org/10.1126/science.1233518

Benson, R. F., Webb, P. A., Green, J. L., Carpenter, D. L., Sonwalkar, V. S., James, H. G., & Reinisch, B. W. (2006). Active wave experiments in space plasmas: The Z mode. In J. W. LaBelle & R. A. Treumann (Eds.), *Geospace electromagnetic waves and radiation* (pp. 3–35). Berlin: Springer. https://doi.org/10.1007/3-540-33203-0_1

Cecconi, B., & Zarka, P. (2005). Direction finding and antenna calibration through analytical inversion of radio measurements performed using a system of two or three electric dipole antennas on a three-axis stabilized spacecraft. *Radio Science*, *40*, RS3003. https://doi.org/10.1029/2004RS003070

Fischer, G., Cecconi, B., Lamy, L., Ye, S.-Y., Taubenshuss, U., Macher, W., et al. (2009). Elliptical polarization of Saturn kilometric radiation observed from high latitudes. *Journal of Geophysical Research*, *114*, A08216. https://doi.org/10.1029/2009JA014176

Galopeau, P. H. M., Boudjada, M. Y., & Lecacheux, A. (2007). Spectral features of SKR observed by Cassini/RPWS: Frequency bandwidth, flux density and polarization. *Journal of Geophysical Research*, *112*, A11213. https://doi.org/10.1029/2007JA012573

Glauert, S. A., & Horne, R. B. (2005). Calculation of pitch angle and energy diffusion coefficients with the PADIE code. *Journal of Geophysical Research*, *110*, A04206. https://doi.org/10.1029/2004JA010851

Gu, X., Thorne, R. M., Ni, B., & Ye, S.-Y. (2013). Resonant diffusion of energetic electrons by narrowband Z mode waves in Saturn's inner magnetosphere. *Geophysical Research Letters*, *40*, 255–261. https://doi.org/10.1029/2012GL054330

Gurnett, D. A., Kurth, W. S., Hospodarsky, G. B., Persoon, A. M., Averkamp, T. F., Cecconi, B., et al. (2005). Radio and Plasma Wave Observations at Saturn from Cassini's approach and first orbit. *Science*, *307*(5713), 1255. https://doi.org/10.1126/science.1105356

Gurnett, D. A., Kurth, W. S., Kirchner, D. L., Hospodarsky, G. B., Averkamp, T. F., Zarka, P., et al. (2004). The Cassini radio and plasma wave investigation. *Space Science Reviews*, *114*(1-4), 395–463. https://doi.org/10.1007/s11214-004-1434-0

Hamaker, J. P., Bregman, J. D., & Sault, R. J. (1996). Understanding radio polarimetry. I. Mathematical foundations. *Astronomy & Astrophysics, Supplement Series*, *117*(1), 137–147. https://doi.org/10.1051/aas:1996146

Horne, R. B., & Thorne, R. M. (1998). Potential waves for relativistic electron scattering and stochastic acceleration during magnetic storms. *Geophysical Research Letters*, *25*(15), 3011–3014. https://doi.org/10.1029/98GL01002

Horne, R. B., Thorne, R. M., Glauert, S. A., Menietti, J. D., Shprits, Y. Y., & Gurnett, D. A. (2008). Gyro-resonant electron acceleration at Jupiter. *Nature Physics*, *4*(4), 301–304. https://doi.org/10.1038/nphys897

Horne, R. B., Thorne, R. M., Shprits, Y. Y., Meredith, N. P., Glauert, S. A., Smith, A. J., et al. (2005). Wave acceleration of electrons in the Van Allen radiation belts. *Nature Letter*, *437*(7056), 227–230. https://doi.org/10.1038/nature03939

Katoh, Y., Tsuchiya, F., Miyoshi, A., Morioka, H., Misawa, R., Ujiie, W., et al. (2011). Whistler mode chorus enhancements in association with energetic electron signatures in the Jovian magnetosphere. *Journal of Geophysical Research*, *116*, A02215. https://doi.org/10.1029/2010JA016183

Menietti, J. D., Averkamp, T. F., Ye, S.-Y., Horne, R. B., Woodfield, E. E., Shprits, Y. Y., et al. (2015). Survey of Saturn Z-mode emission. *Journal of Geophysical Research: Space Physics*, *120*, 6176–6187. https://doi.org/10.1002/2015JA021426

Morooka, M. W., Modolo, R., Wahlund, J.-E., André, M., Eriksson, A. I., Persoon, A. M., et al. (2009). The electron density of Saturn's magnetosphere. *Annales Geophysique*, *27*(7), 2971–2991. https://doi.org/10.5194/angeo-27-2971-2009

Persoon, A. M., Kurth, W. S., Gurnett, D. A., Groene, J. B., Sulaiman, A. H., Wahlund, J.-E., et al. (2018). Electron-density distributions in Saturn's ionosphere. *Geophysical Research Letters*, *45*. https://doi.org/10.1029/2018GL078020

Reeves, G. D., Spence, H. E., Henderson, M. G., Morley, S. K., Friedel, R. H. W., Funsten, H. O., et al. (2013). Electron acceleration in the heart of the Van Allen radiation belts. *Science*, *341*(6149), 991–994. https://doi.org/10.1126/science.1237743

Shprits, Y. Y., Elkington, S. R., Meredith, N. P., & Subbotin, D. A. (2008). Review of modeling of losses and sources of relativistic electrons in the outer radiation belt I: Radial transport. *Journal of Atmospheric and Solar - Terrestrial Physics*, *70*(14), 1679–1693. https://doi.org/10.1016/j.jastp.2008.06.008

Shprits, Y. Y., Menietti, J. D., Gu, X., Kim, K.-C., & Horne, R. B. (2012). Gyro-resonant interactions between the radiation belt electrons and whistler mode chorus waves in the radiation environments of Earth, Jupiter, and Saturn, a comparative study. *Journal of Geophysical Research*, *117*, A11216. https://doi.org/10.1029/2012JA018031

Shprits, Y. Y., Subbotin, D. A., Meredith, N. P., & Elkington, S. R. (2008). Review of modeling of losses and sources of relativistic electrons in the outer radiation belt II: Local acceleration and loss. *Journal of Atmospheric and Solar - Terrestrial Physics*, *70*(14), 1694–1713. https://doi.org/10.1016/j.jastp.2008.06.014

Stix, T. H. (1992). *Waves in plasmas* (p. 22). New York, NY: American Institute of Physics.

Sulaiman, A. H., Kurth, W. S., Persoon, A. M., Menietti, J. D., Farrell, W. M., Ye, S.-Y., et al. (2017). Intense harmonic emissions observed in Saturn's ionosphere. *Geophysical Research Letters*, *44*, 12,049–12,056. https://doi.org/10.1002/2017GL076184

Wahlund, J.-E., Boström, R., Gustafsson, G., Gurnett, D. A., Kurth, W. S., Averkamp, T., et al. (2005). The inner magnetosphere of Saturn: Cassini RPWS cold plasma results from the first encounter. *Geophysical Research Letters*, *32*, L20S09. https://doi.org/10.1029/2005GL022699

Wahlund, J.-E., Morooka, M. W., Hadid, L. Z., Persoon, A. M., Farrell, W. M., Gurnett, D. A., et al. (2018). In situ measurements of Saturn's ionosphere show it is dynamic and interacts with the rings. *Science*, *359*(6371), 66–68. https://doi.org/10.1126/science.aao4134

Woodfield, E. E., Horen, R. B., Glauert, S. A., Menietti, J. D., & Shprits, Y. Y. (2016). A new source region for Saturn's inner electron radiation belts, Presented at the American Geophysical Union Meeting, SM43D-06, Dec. 15, 2016, San Francisco, CA.

Woodfield, E. E., Horne, R. B., Glauert, S. A., Menietti, J. D., & Shprits, Y. Y. (2014). The origin of Jupiter's outer radiation belt. *Journal of Geophysical Research: Space Physics*, *119*, 3490–3502. https://doi.org/10.1002/2014JA019891

Wu, C. S., & Lee, L. C. (1979). A theory of the terrestrial kilometric radiation. *The Astrophysical Journal*, *230*, 621–626. https://doi.org/10.1086/157120

Ye, S.-Y., Menietti, J. D., Fischer, G., Wang, Z., Cecconi, B., Gurnett, D. A., & Kurth, W. S. (2010). Z mode waves as the source of Saturn narrowband radio emissions. *Journal of Geophysical Research*, *115*, A08228. https://doi.org/10.1029/2009JA015167